# FIELD TEST RESULTS OF A PV-HVAC SYSTEM WITH PCM-STORAGE FOR IMPROVED GRID INTERACTION

**Richard Schex[1], Andreas Krönauer[1], Simon Pöllinger[1], Stefanie Tafelmeier[1], Timo Korth[2], Felix Loistl[2], Christian Schweigler[2]**

[1] Bavarian Center of Applied Energy Research (ZAE Bayern), Garching (Germany)

[2] CENERGIE, Munich University of Applied Sciences, Munich (Germany)

## Abstract

This paper presents the key results of the development and successful integration of a PCM (phase change material) storage to a solar-electric driven air conditioning system (PV-HVAC). The main goals are to increase self-consumption, reduce electrical peak load demand and feed-in peaks by the PV plant. In this paper the benefits of the storage integration in terms of system efficiency, solar-fraction and reduction of electrical peak demand are described. For verification the PV-HVAC system without storage was evaluated the entire cooling period 2018. The PCM-storage was integrated and the system is analyzed in the cooling period 2019. Results of the pilot installation will confirm storage function under real terms of operation. Long term measurements allow a detailed and very reliable comparison between the operation with and without storage. To optimize storage usage, predictive storage control strategies had been implemented and will be discussed.

*Keywords: Air conditioning, Variable refrigerant flow (VRF), Phase change material (PCM), Thermal storage, PV-self-consumption, Demand side management, Predictive control strategy*

**Nomenclature**

| | | | | | |
|---|---|---|---|---|---|
| $d$ | Distance [m] | $Q$ | Thermal energy [kWh] | $Feed\ in$ | Electrical grid feed in |
| $DEER$ | Daily EER [-] | $\dot{Q}$ | Thermal power [kW] | $Gen$ | Generation |
| $E$ | Electrical energy [kWh] | $SoC$ | State of charge [%] | $Grid$ | Electrical grid |
| $\dot{E}$ | Electrical power [kW] | $ST$ | Storage | $HP$ | High pressure |
| $ECO$ | Economizer | $T$ | Temperature [°C] | $IU$ | Indoor units |
| $EER$ | Energy efficiency ratio [-] | $t$ | Time | $LP$ | Low pressure |
| $H$ | (Time) Horizon | $VRF$ | Variable refrigerant flow | $LQ$ | Liquid |
| $h$ | Enthalpy [kJ/kg] | $x$ | Steam fraction [%] | $max, min$ | Maximum, Minimum |
| $HEX$ | (Air) heat exchanger | $\lambda$ | Calculation parameter | $OU$ | Outdoor Unit |
| $HVAC$ | Heating, ventilation and cooling | Indices | | $Ref$ | Refrigerant |
| $\dot{m}$ | Mass flow [kg/h] | $Amb$ | Ambient | $Res$ | Residual |
| $P$ | Pressure [bara] | $Cons$ | Consumption | $set$ | Setpoint |
| $PCM$ | Phase change material | $Evap$ | Evaporation | $Sys$ | System |
| $PV$ | Photovoltaik [kWp] | $Ex$ | Excess | $1, 2$ | Inlet, Outlet |

## 1. Introduction

An increasing use of renewable energy sources requires efficient and economical solutions for storing energy. Especially for heating and cooling purposes, storages based on phase change material (PCM) seem to have a high potential. To be economically competitive to other storage technologies, like electrochemical storages, it is mandatory to design specific storage solutions which are well adapted to the application. Therefore a new approach was chosen where a PCM-storage is charged and discharged via refrigerant instead using a separate brine loop. The thermal behavior of the storage was validated by laboratory investigation (Korth et al., 2018) and is now applied in a Variable Refrigerant Flow heating and cooling system (VRF) for a proof of concept. The entire system is driven by the electrical output of a PV generator and by the electrical grid.

For proper system design in a realistic field installation, a specific heating and cooling system had been modeled in detail. The system supplies laboratories and offices in a non-residential building in the south of Germany. Several storage configurations and implementations were evaluated. One of the most promising designs has finally been built up. The entire system is characterized by the following key sizing parameters.

- Systems thermal cooling capacity: 22.4 kW
- Electrical system load at nominal operation: 5.5 kW
- Size of PV-generator: 7.2 kWp
- Latent heat content of the PCM-storage: 14 kWh
- Thermal storage power capacity at average state of charge (SoC): 5 kW
- Storage material: Paraffin graphite compound, nominal melting temperature of 18 °C


doi:10.18086/swc.2019.55.12 Available at http://proceedings.ises.org

The design process as well as the storage implementation is described in detail in a previous SHC paper (Schex et al., 2017). Main aspects are summarized in the following subsections.

## 2. Methodology

### 2.1. Measurement concept/data acquisition

After the system design phase had been completed, the pilot installation has been built up. A measurement concept has been set up which allows an entire and detailed system evaluation.

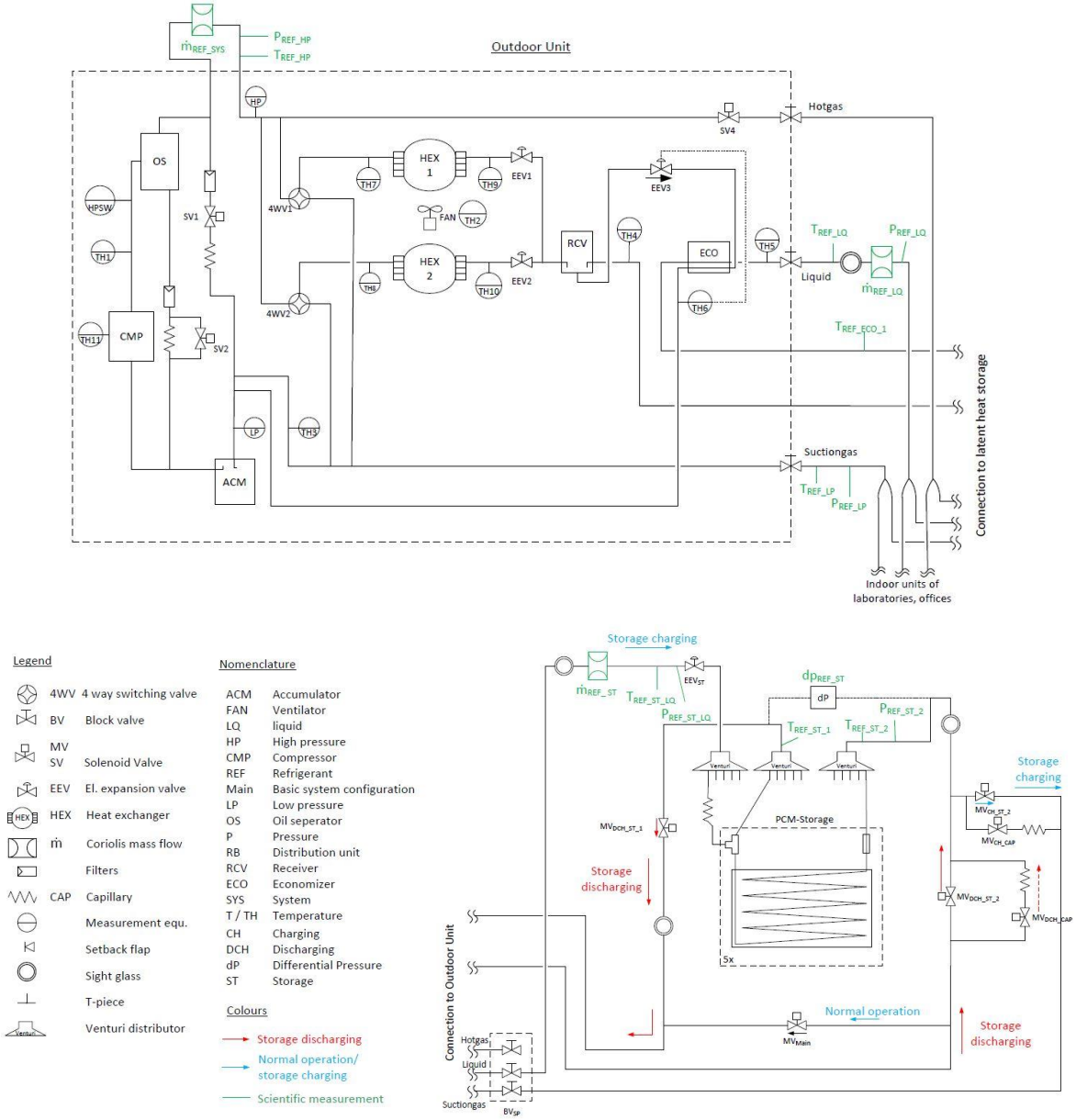


**Figure 1: Systems P&ID including outdoor unit, storage connection and measurement equipment of the pilot installation.**

The top section of Figure 1 shows the outdoor unit of the VRF system (Swegon, 2014). On its right side the connection to the thermal storage is displayed. The storage itself is shown in the bottom part of Figure 1. Blue arrows indicate the refrigerants flow in case of normal operation or in storage charging mode. During charging, the storage works as additional load, comparable to an indoor unit operated as evaporator. The red arrows indicate the refrigerant flow for storage discharge. The storage subcools the condensed refrigerant. All green parts indicate scientific measurement equipment to evaluate the system. Temperature, pressure and mass flow are measured in direct contact to the refrigerant. Thus, specific enthalpy of the refrigerant for each state point of the cycle can be determined.

Figure 2 shows exemplarily the measured data points to determine the energy balance of the outdoor unit and the PCM-storage.

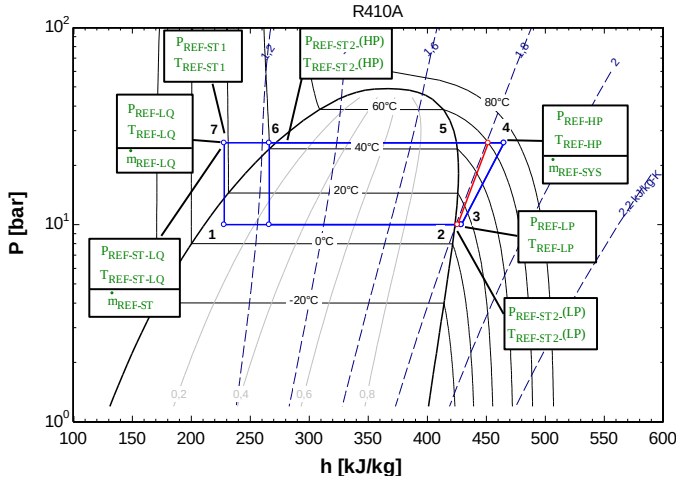


**Figure 2: Log(p)/h diagram showing measured data points for energy balancing.**

Based on constantly measured data, the systems cooling capacities as well as the storage charging and discharging capacity are calculated by the following equations 1-3. In the same way all other thermal capacities are calculated to get a valid thermal energy balance.

$$\dot{Q}_{Charge} = \dot{m}_{Ref,ST} * (h_{Ref,ST,2} - h_{Ref,ST,LQ}) \quad \text{(eq. 1)}$$

$$\dot{Q}_{Disch} = \dot{m}_{Ref,LQ} * (h_{Ref,ST,2} - h_{Ref,ST,1}) \quad \text{(eq. 2)}$$

$$\dot{Q}_{Evap,Cycle} = \dot{m}_{Ref,LQ} * (h_{Ref,LP} - h_{Ref,LQ}) \quad \text{(eq. 3a)}$$

$$\dot{Q}_{Evap,Load} = \dot{Q}_{Evap,Cycle} - \dot{Q}_{Charge} \quad \text{(eq. 3b)}$$

$\dot{Q}_{Evap,Cycle}$ (eq. 3a) represents the entire system power capacity, a temporary storage charging included. $\dot{Q}_{Evap,Load}$ (eq. 3b) represents the used thermal capacity in all indoor units of the VRF-system. In case of regular operation (nether charging or discharging takes place) or storage discharging this capacity is equal to $\dot{Q}_{Evap,Cycle}$. Only in storage charging mode, when part of the entire cycle capacity is used to charge the storage $\dot{Q}_{Evap,Load}$ is lower than $\dot{Q}_{Evap,Cycle}$.

Based on thermal and electrical data, system efficiencies and a daily EER (DEER) are defined:

$$EER_{Cycle} = \frac{\dot{Q}_{Evap,Cycle}}{\dot{E}_{Cons,Sys}} = \frac{\dot{Q}_{Evap,Cycle}}{\dot{E}_{OU}+\dot{E}_{IU}+\dot{E}_{ST}} \quad \text{(eq. 5a)}$$

$$EER_{Load} = \frac{\dot{Q}_{Evap,Load}}{\dot{E}_{Cons,Sys}} = \frac{\dot{Q}_{Evap,Load}}{\dot{E}_{OU}+\dot{E}_{IU}+\dot{E}_{ST}} \quad \text{(eq. 5b)}$$

$$DEER = \int_{0h}^{24h} \frac{\dot{Q}_{Evap,Load}(t)}{\dot{E}_{Cons,Sys}(t)} dt \quad \text{(eq. 6)}$$

Consequently to equation 3a and 3b the EER is distinguished by a $EER_{Cycle}$ (storage charging capacity included, eq. 5a) and a $EER_{Load}$ (only used capacity of the indoor units, eq. 5b). Both EER values are calculated using the entire electrical power consumption of the system. Electrical power includes the compressor and all other components of the outdoor unit, the indoor units as well as auxiliary power to run the storage.

Equation 6 defines a daily efficiency DEER. It describes the ratio of generated cooling energy used in the indoor units to the entirely consumed electrical energy on a daily basis.

The systems evaluation takes place continuously during real operation of the system. Therefore, a validity check of the measured data has to be applied. E.g. cooling data are only assumed to be valid when the condensed refrigerant is liquefied to 100%. This ensures stable and valid states for enthalpy as well as a reliable measurement of the refrigerant mass flow $\dot{m}_{Ref}$.

2.2. Analysis of reference operation during cooling period 2018

In the cooling period 2018 the conventional VRF-system without using the thermal storage has been evaluated.

**Table 1: Measured reference EER data (mean values). Sorted by different ambient temperature and part load ranges.**

| $EER_{Load}$ [-] | | Ambient temperature [°C] | | | | | | | | | | |
|---|---|---|---|---|---|---|---|---|---|---|---|---|
| | | 0-15 | 15-17 | 17-19 | 19-21 | 21-23 | 23-25 | 25-27 | 27-29 | 29-31 | 31-33 | 33-40 |
| $\dot{Q}_{Evap,Load}$ | 0,1-6 | 2,17 | 2,48 | 2,39 | 2,55 | 2,68 | 2,75 | 2,80 | 2,79 | 2,58 | -- | -- |
| | 6-10 | 3,43 | 3,48 | 3,47 | 3,51 | 3,53 | 3,48 | 3,41 | 3,42 | 3,36 | 3,24 | 3,13 |
| | 10-14 | 3,74 | 3,84 | 3,89 | 3,86 | 3,82 | 3,74 | 3,56 | 3,47 | 3,52 | 3,41 | 3,12 |
| | 14-18 | 4,00 | 3,66 | 3,91 | 3,91 | 3,83 | 3,73 | 3,66 | 3,63 | 3,47 | 3,27 | 3,04 |
| | 18-24 | -- | -- | -- | 3,40 | 3,74 | 3,50 | 3,56 | 3,49 | 3,37 | 3,19 | 3,00 |

Table 1 shows the mean EER values for specific ambient temperatures and part load conditions. Only operation states with a significant amount of occurrence are presented. Therefore, for the extreme constellations (e.g. low part load at high ambient temperature and vice versa) no data are given. The recorded data are used as reference for analysis of the system working with thermal storage. A curve fitting method has been applied in order to obtain a continuous relation for the EER as function of ambient temperature and part load state. It is used to improve the systems model (Schex et al., 2017) and is further applied for the comparison of the system solar operation with and without storage in chapter 3.4.

2.3. Solar operation

To evaluate the use of solar energy by the PV-driven VRF system with PCM-storage, the ratios of autarky and self-consumption are applied (Weniger et al., 2015).

$$Autarky\ rate = \frac{E_{Cons,Sys} - E_{Grid}}{E_{Cons,Sys}} \quad \text{(eq. 7)}$$

$$Self\ consumption\ rate = \frac{E_{Gen,PV} - E_{Feed\ in}}{E_{Gen,PV}} \quad \text{(eq. 8)}$$

Equation 7 indicates the share of the electrical energy consumption which is satisfied by onsite PV-generation. Remaining energy demand is taken from the electrical grid. Equation 8 shows the self-consumption rate of the onsite PV-generation. Surplus PV-yield which is not used on site is fed into the electrical grid. Both parameters are on the contrary. For a grid orientated system design both parameter need to be taken into account.

To assess the grid interaction, i.e. the effect of the PV-driven cooling system on the stability of the electrical grid, the power exchange has to be analyzed with a high temporal resolution. For this purpose data of the electrical demand of the system, of the PV generation, and the power exchanged with the grid are recorded (sampling rate 4 sec.) and sorted according to their relative occurrence. When a reduction of the grid interaction shall be accomplished, the occurrence of states with low power exchange with the grid is to be strengthened.

2.4. Storage control strategy

During charging the storages operates like an evaporator. An evaporator is usually controlled via expansion valve and its set point of superheat for the vaporized refrigerant. To integrate properly solar energy of the PV generator, this control strategy has to be changed. First the output of the PV generator is used to fulfil the systems thermal load. When PV solar output is higher than the electrical demand of the HVAC system, the charging strategy is governed by the difference of solar yield and system demand. Simultaneously stable superheat of the refrigerant leaving the evaporator has to be ensured at any time. Temporarily minor losses of efficiency are inevitable due to excessive high superheat. Storage discharge starts when the solar yield falls below the systems demand, usually in the afternoon.

Further on this relatively simple strategy is called “maximized self-consumption”. It already ensures an increase of solar fraction. Yet, if the grid interaction of the system shall be further minimized, predictive control strategies need to be implemented. Therefore, different strategies were considered. Finally a strategy based on Braam et al., 2014 has been selected. Originally this strategy has been developed for PV-battery systems. Where necessary for the operation of the PCM-storage, the strategy has been adapted.

The prediction is primarily based on recorded data. That means the load and generation trends, e.g. of the

preceding working day, are used for an estimation of the expected charging capacity. In equation 9 the residual electrical excess energy $E_{Res}^{Ex}(t)$ over the forecasted horizon H is calculated. Its maximum occurs for t = 0, approaching zero for t = H. This electrical excess energy trend is transformed to a thermal energy $Q_{Res}^{Ex}(t)$ by the expected mean EER (equation 10). In a last step (equation 11) a time schedule for the loading of the storage, expressed by target values for the state of charge $SoC_{set}(t)$ is calculated.

$$E_{Res}^{Ex}(t) = \int_{t}^{t+H} max\,(0,\ \dot{E}_{Gen,PV}(t') - \dot{E}_{Cons,Sys}(t'))dt' \quad \text{(eq. 9)}$$

$$Q_{Res}^{Ex}(t) = E_{Res}^{Ex}(t) * \overline{EER} \quad \text{(eq. 10)}$$

$$SoC_{set}(t) = \max(1 - \lambda \frac{Q_{Res}^{Ex}(t)}{Q_{Storage}^{Total}}, SoC_{min}) \quad \text{(eq. 11)}$$

$SoC_{set}(t)$ depends, besides $Q_{Res}^{Ex}(t)$, on the nominal storage capacity $Q_{Storage}^{Total}$, the calculation parameter λ and $SoC_{min}$. The parameter λ from 1 to 0 varies the calculated course of $SoC_{set}(t)$. $SoC_{min}$ limits the lower boundary of the starting set point (Braam et al., 2014).

During operation $SoC_{set}$ is compared to the measured SoC. If the current SoC value is higher than $SoC_{set}$ the operation mode is changing from "maximized self-consumption" to a "peak-shaving" mode. In that mode, not the entire PV-surplus is used for storage charging. Instead a specified value of PV feed-in is accepted. Usable storage capacity will be restrained. If $Q_{Res}^{Ex}$ is lower than expected, e.g. due to lower PV-yield, the trend line of $SoC_{set}$ should remain above the measured SoC. "Maximized self-consumption" will be applied and no loss of solar fraction is expected.

For all upcoming SoC data 100% mean that PCM is completely solid, 0% mean that it is liquid. To apply the explained strategy a reliable real time measurement of the SoC is mandatory. As Helm et al, 2013 shows, the measurement of latent heat storages SoC can be very complex. For that reason, details of the measurement procedure are not subject of this paper, but the working principle is briefly described.

The density of the PCM in solid and liquid state differs, hence the volume changes. Due to the volume change the PCM surface level inside the storage varies. The actual PCM level is measured by an ultrasonic sensor. The sensor provides a signal according to the distance between the storage cover and the momentary PCM level. If the PCM is fully liquid (SoC 0%), the distance is the smallest and vice versa. The used correlation between the distance d and the SoC is simplified to a linear regression (equation 12).

$$SoC_{measure} = 13.286\,d - 79.413 \quad \text{(eq. 12)}$$

The graphite filling in the PCM compound limits the measurement, because the PCM level during crystallization falls below the graphite surface. This happens when the storage reaches a SoC of 80% and higher. Hence, SoC values above 80% cannot be expressed by means of the measured distance.

## 3. Results

### 3.1. Storage start up

After completion of the thermal storage design, a demonstrator with reduced storage capacity has been built up. It has been tested on a refrigeration test cycle (Korth et al., 2018). After successful testing, a full-size pilot storage has been constructed with minor adaptions with respect to the VRF-system. One important goal of the storage implementation is to maintain systems cycle efficiency during charging of the storage. Therefore, the storage is charged by refrigerant evaporation at the common system evaporation temperature level. During the discharging phase an efficiency boost is achieved allowing for a lower electrical demand when appropriate.

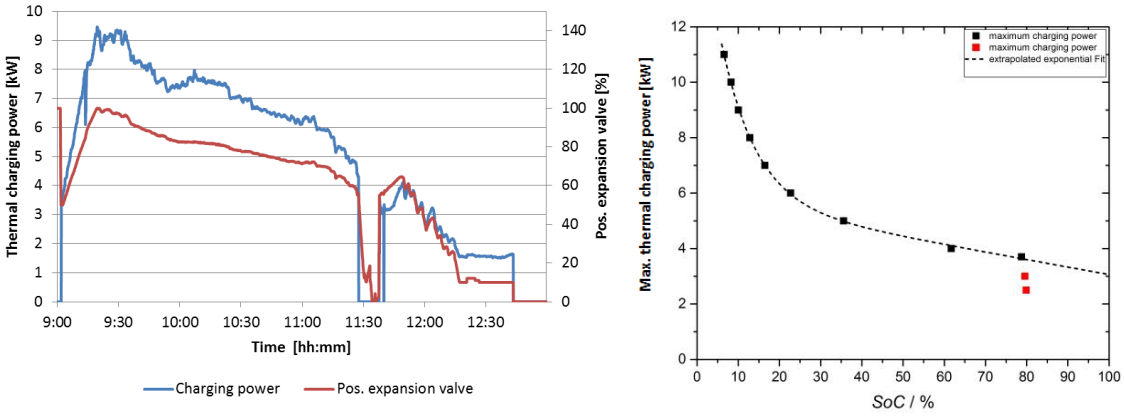


**Figure 3: Entire charging cycle controlled by heat exchanger outlet superheat (left). Modeled power capacity of the storage (right).**

Figure 3 (left) shows one entire charging cycle of the pilot storage. At 09:00 the storage is completely liquid (SoC=0%). The electronic expansion valve ($EEV_{ST}$) controlling the refrigerant flow through the storage is controlled with regard to the superheat of the refrigerant at heat exchanger outlet. Therefore the blue line represents the maximum possible charging power at every time step. The charging interruption at 11:30 is due to an oil recovery cycle of the VRF-system. Charging ends when the phase change is completed (SoC=100 %) indicated by a strong decline of the charging capacity. Finally, when the PCM volume is cooled below the phase change temperature, also some sensible heat is stored.

The typical characteristic of a storage based on PCM is perceptible. At the beginning of the charging process the highest power capacity is reached from 8 to 9 kW. In the middle part of the charging process, during solidifying, the PCM-storage capacity reaches 5 to 7.5 kW. This typical behavior is due the growing solid phase front around the heat exchanger which reduces the thermal conductivity which is the reason for the decreasing thermal capacity. At the very end of the charging process the capacity drops down to 2 kW, because most of the PCM is already solid.

Figure 3 (right) shows the expected behavior, based on the model developed during storage design phase (Schex et al., 2017). The curve fit represents the maximum possible thermal capacity for a rising state of charge. The red dots are showing the predicted breakdown of the storage capacity for high SoC. They are not taken into account of the extrapolation. Between a SoC of 20 and 60% a thermal power from 6 to 4 kW has been predicted. Based on practical results, the pilot storage delivers an even higher capacity in that SoC range. The main reason for the difference should be the thermal conductivity of the paraffin graphite compound, which had been underestimated during the design phase.

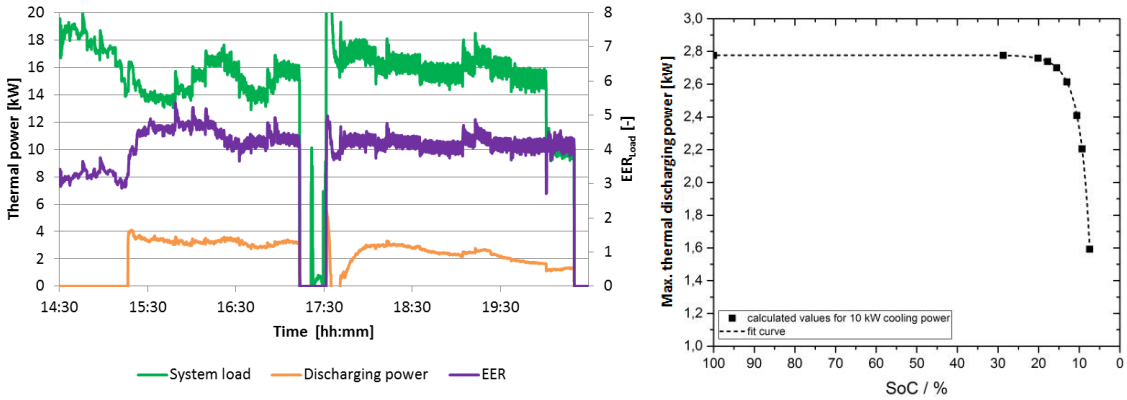


**Figure 4: Discharging cycle. VRF system load (green), discharging power (orange). Resulting systems EER (purple) (left graph). Modeled power capacity of the storage discharging (right graph).**

Figure 4 (left) shows an entire discharging cycle. At the beginning the storage is entirely solid (SoC=100%). In this mode the latent heat storage serves as a subcooler for the refrigerant leaving the air heat exchanger (HEX) of the outdoor unit in which condensation of the refrigerant takes place. Discharging is continued until each of the four installed internal temperature sensors of the PCM is indicating a temperature higher than the melting

temperature of 18 °C. The SoC drops constantly from 100 to 0%. The discharging starts at 15:15 and is interrupted at 17:15 because of an oil recovery cycle of the VRF-system. When the system starts up again at 17:30, for a period of 20 to 30 min the function of the storage deviates from the intended sub-cooler effect. In this phase, due to insufficient condensation of refrigerant in the HEX, the storage provides additional condensation capacity. In this moment, analysis of the refrigerant data yield incorrect results for the PCM-storage. Thus, in contrary to the course of the discharging capacity shown in Figure 5, a rather high cooling capacity is provided by the storage for that period of time.

The system´s $EER_{Load}$ (purple, second y-Axis) is slightly higher than 3, before storage discharge starts (14:30–15:15). When storage discharge begins, the $EER_{Load}$ steps up to 4 and above for the entire discharging cycle. The share of cooling output during discharging related to the total cooling output of the system varies between 11 and 26%. Most of the time the share is higher than 20%, which causes the significant $EER_{Load}$ boost.

The right side of Figure 4 shows an exemplary plot of the storage discharging behavior from the design phase. The black curve shows the SoC-dependent discharge power for an exemplary system load of 10 kW. For an assumed storage inlet temperature of 48 °C, about 28% of cooling power can be taken out of the storage. In case of discharge the heat transfer inside the storage is not limiting the system, and discharging power is widely independent from the SoC or the system load. Only at the very end of discharging (SoC<20%), the available capacity is going down.

3.2. Storage charging data

All data discussed in this section have been gained from 17th of April to 31st of July 2019. They are used to compare the system during charging operation with the system in "regular operation", where neither charging nor discharging takes place. The system worked in solar operation mode. The electronic expansion valve ($EEV_{ST}$) responsible for the charging capacity was regulated according to current PV surplus energy.

**Table 2: System data gained from 17th of April to 31st of July 2019. Comparison of storage charging to regular operation.**

| $EER_{Load}$ [-] | | Ambient temperature [°C] | | | | | | | | | | |
|---|---|---|---|---|---|---|---|---|---|---|---|---|
| | | 0-15 | 15-17 | 17-19 | 19-21 | 21-23 | 23-25 | 25-27 | 27-29 | 29-31 | 31-33 | 33-40 |
| $\dot{Q}_{Evap,Load}$ (regular operation) | 0,1-6 | 2,06 | 2,06 | 2,16 | 2,12 | 2,20 | 2,16 | 2,54 | 2,45 | 2,65 | -- | -- |
| | 6-10 | 3,59 | 3,58 | 3,56 | 3,42 | 3,48 | 3,50 | 3,54 | 3,56 | 3,38 | 3,38 | 3,29 |
| | 10-14 | -- | -- | 4,12 | 3,94 | 3,87 | 3,83 | 3,82 | 3,76 | 3,79 | 3,65 | 3,56 |
| | 14-18 | -- | -- | -- | -- | -- | 3,88 | 3,74 | 3,71 | 3,68 | 3,57 | 3,31 |
| | 18-24 | -- | -- | -- | -- | -- | -- | -- | -- | 3,57 | 3,48 | 3,24 |
| $EER_{Cycle}$ [-] | | Ambient temperature [°C] | | | | | | | | | | |
| | | 0-15 | 15-17 | 17-19 | 19-21 | 21-23 | 23-25 | 25-27 | 27-29 | 29-31 | 31-33 | 33-40 |
| $\dot{Q}_{Evap,Cycle}$ (incl. charging) | 0,1-6 | -- | 2,23 | 2,44 | 2,74 | 2,73 | 2,67 | -- | -- | -- | -- | -- |
| | 6-10 | -- | -- | 3,69 | 3,74 | 3,68 | 3,71 | 3,72 | 3,53 | 3,41 | 3,52 | -- |
| | 10-14 | -- | -- | 4,28 | 4,20 | 4,02 | 4,04 | 3,94 | 3,80 | 3,75 | 3,75 | -- |
| | 14-18 | -- | -- | 4,33 | 4,33 | 4,24 | 4,07 | 3,93 | 3,84 | 3,66 | 3,59 | 3,30 |
| | 18-24 | -- | -- | -- | -- | 4,14 | 4,07 | 3,89 | 3,86 | 3,69 | 3,54 | 3,33 |
| Rel. change [%] | | Ambient temperature [°C] | | | | | | | | | | |
| | | 0-15 | 15-17 | 17-19 | 19-21 | 21-23 | 23-25 | 25-27 | 27-29 | 29-31 | 31-33 | 33-40 |
| $\dot{Q}_{Evap}$ | 0,1-6 | -- | 0,08 | 0,13 | 0,29 | 0,25 | 0,24 | -- | -- | -- | -- | -- |
| | 6-10 | -- | -- | 0,04 | 0,09 | 0,06 | 0,06 | 0,05 | -0,01 | 0,01 | 0,04 | -- |
| | 10-14 | -- | -- | 0,04 | 0,07 | 0,04 | 0,06 | 0,03 | 0,01 | -0,01 | 0,03 | -- |
| | 14-18 | -- | -- | -- | -- | -- | 0,05 | 0,05 | 0,04 | -0,01 | 0,00 | 0,00 |
| | 18-24 | -- | -- | -- | -- | -- | -- | -- | -- | 0,03 | 0,02 | 0,03 |

Table 2 shows a matrix of mean EER values clustered by different ambient temperature and part load ranges in analogy to Table 1. The first section shows the system efficiency in regular operation. The storage was already integrated but no charging or discharging happens. $EER_{Load}$ defined in equation 5b is obtained for the reference case, but $EER_{Cycle}$ would show the same data because no storage charging happens. The middle part indicates the mean EER when the system is working and the storage is charged simultaneously. In order to evaluate the storage effect on system efficiency during charging $EER_{Cycle}$ (eq. 5a) is used. It is formed by the ratio of cooling output to entire electrical system demand. Heat extraction here is regarded as a part of the generated cooling capacity.

The last matrix shows the relative difference from the charging process compared to the regular operation. A positive value means cycle efficiency improvement for the operation with storage. Only data where both sections offer sufficient data are compared.

As charging is realized on the common system´s evaporation temperature level, no negative effects on the cycle EER are expected. Data above 10 kW load respectively over 27 °C ambient temperature prove this expectation. For low part load ratios below 10 kW even an increase of the cycle efficiency is reached. The storage causes a more constant operation for the low part load regime, which leads to higher mean efficiency values. The charging process is at least realized at the same efficiency the regular system is capable to perform.

3.3. Storage discharging data

Data acquisition is done in the same time period and the same methodology as described in the prior subsection. Now the storage discharging phases are compared to regular operation. Discharging takes place when the electrical system load is higher than PV-yield, which usually occurs in the morning or in the afternoon hours.

**Table 3: System data from 17th of April to 31st of July 2019. Comparison of storage discharging to regular operation.**

| $EER_{Load}$ [-] | | Ambient temperature [°C] | | | | | | | | | | |
|---|---|---|---|---|---|---|---|---|---|---|---|---|
| | | 0-15 | 15-17 | 17-19 | 19-21 | 21-23 | 23-25 | 25-27 | 27-29 | 29-31 | 31-33 | 33-40 |
| $\dot{Q}_{Evap,Load}$ (regular operation) | 0,1-6 | 2,06 | 2,06 | 2,16 | 2,12 | 2,20 | 2,16 | 2,54 | 2,45 | 2,65 | -- | -- |
| | 6-10 | 3,59 | 3,58 | 3,56 | 3,42 | 3,48 | 3,50 | 3,54 | 3,56 | 3,38 | 3,38 | 3,29 |
| | 10-14 | -- | -- | 4,12 | 3,94 | 3,87 | 3,83 | 3,82 | 3,76 | 3,79 | 3,65 | 3,56 |
| | 14-18 | -- | -- | -- | -- | -- | 3,88 | 3,74 | 3,71 | 3,68 | 3,57 | 3,31 |
| | 18-24 | -- | -- | -- | -- | -- | -- | -- | -- | 3,57 | 3,48 | 3,24 |
| $EER_{Load}$ [-] | | Ambient temperature [°C] | | | | | | | | | | |
| | | 0-15 | 15-17 | 17-19 | 19-21 | 21-23 | 23-25 | 25-27 | 27-29 | 29-31 | 31-33 | 33-40 |
| $\dot{Q}_{Evap,Load}$ (incl. discharge) | 0,1-6 | 2,59 | 2,54 | 2,61 | 2,73 | 2,20 | 2,67 | 2,72 | 2,69 | -- | -- | -- |
| | 6-10 | 3,61 | 3,88 | 3,73 | 3,81 | 3,83 | 3,86 | 3,98 | 3,96 | 3,98 | 3,83 | -- |
| | 10-14 | -- | -- | 4,59 | 4,43 | 4,47 | 4,31 | 4,38 | 4,23 | 4,19 | 4,28 | 4,19 |
| | 14-18 | -- | -- | -- | -- | 4,73 | 4,51 | 4,39 | 4,49 | 4,43 | 4,39 | 4,19 |
| | 18-24 | -- | -- | -- | -- | -- | -- | -- | -- | 4,43 | 4,24 | 4,11 |
| Rel. change [%] | | Ambient temperature [°C] | | | | | | | | | | |
| | | 0-15 | 15-17 | 17-19 | 19-21 | 21-23 | 23-25 | 25-27 | 27-29 | 29-31 | 31-33 | 33-40 |
| $\dot{Q}_{Evap}$ | 0,1-6 | 0,26 | 0,23 | 0,21 | 0,29 | 0,00 | 0,24 | 0,07 | 0,10 | -- | -- | -- |
| | 6-10 | 0,01 | 0,09 | 0,05 | 0,11 | 0,10 | 0,10 | 0,13 | 0,11 | 0,18 | 0,13 | -- |
| | 10-14 | -- | -- | 0,11 | 0,12 | 0,16 | 0,12 | 0,14 | 0,13 | 0,10 | 0,17 | 0,18 |
| | 14-18 | -- | -- | -- | -- | -- | 0,16 | 0,17 | 0,21 | 0,20 | 0,23 | 0,27 |
| | 18-24 | -- | -- | -- | -- | -- | -- | -- | -- | 0,24 | 0,22 | 0,27 |

During storage discharge a significant part of cooling load is contributed by the PCM-storage in order to lower the electrical system demand. Table 3 shows the previously established part load and ambient temperature matrix. Now system operation during discharging (middle part) is compared to regular operation (upper part). In both cases the definition of $EER_{Load}$ (eq. 5b) is used.

Relative improvement is shown in the last matrix. For the reasoning of the reached EER-boost compared to the reference, differentiation between the different load states has to be made. For low part load ratios, EER gains of more than 20% are reached. In this specific part load area only one air heat exchanger (HEX 1) of the VRF system is working. The expansion valve of HEX 1 is functioning as a flow valve and restricts the refrigerant in order to maintain the high pressure level. Refrigerant at a high temperature level leaves the HEX 1 and enters the PCM-storage. The storage is able to provide a relatively high subcooling capacity. For the middle part load area the storage only reaches EER-gains from 10 to 16% (when $T_{Amb}$ is higher than $T_{PCM}$=18 °C). In this part of operation the second air heat exchanger HEX 2 starts. If system load is high enough to maintain the high pressure level, the two air heat exchangers are able to cool down the refrigerant close to the ambient temperature. This causes a relatively low storage inlet temperature, depending on $T_{Amb}$. Thus, the effect of cooling the refrigerant by heat transfer to the storage is limited. Whereas, working at high part load ratios respectively high ambient temperatures the storage has its most significant effect. EER benefits from 20 to 27% are achieved. For high ambient temperatures, when air-air based systems are struggling for efficiency, the storage boosts efficiency as desired.

3.4. Storage solar operation

For solar operation a comparison to the 2018´s data does not seem to be adequate. Boundary conditions are varying too much and a mix of different boundary conditions does not guarantee a valid output. Therefore an assessment based on exemplary type days in 2019 had been selected.

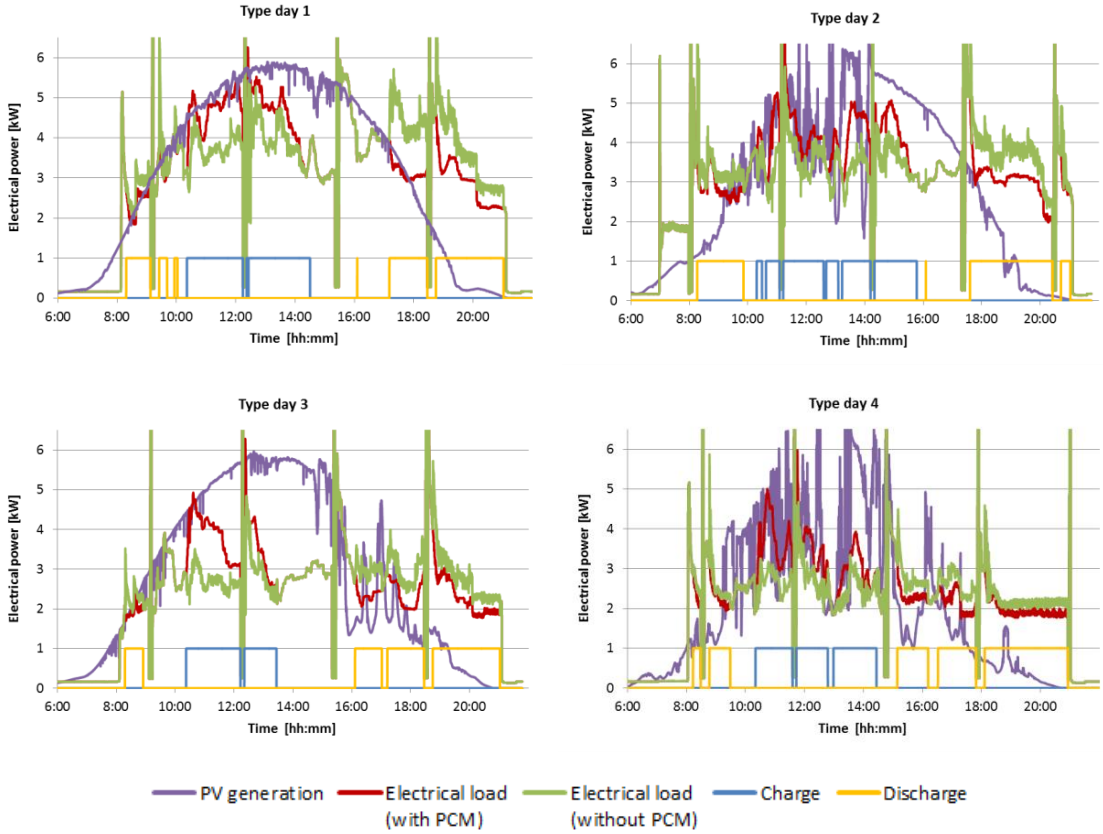


**Figure 5: Four representative type days. PV yield (violet), Electrical system load with PCM (red) and without PCM (green).**

Figure 5 shows the representative type days, selected from operation data 2019. Solar excess energy needed to be high enough to ensure an entire charging cycle. The type days are classified as follows:

1. Clear sky, sunny day with high system load (left top).
2. Partly scattered clouds with high system load (right top).
3. Partly scattered clouds with average system load (left bottom).
4. Scattered clouds with average to low system load (right bottom).

Each violet trend shows the measured electrical generation of the PV-plant. The red line indicates the measured electrical load of the entire system. The binary data in yellow and blue are indicating, weather the storage was in charging or in discharging operation. For time steps in between, the storage wasn´t operating at all.

The green line indicates how the system would have worked without the storage. In times without usage of the storage, identical performance is assumed for the system without (green) and with storage (measured data, red). In times of storage charging or discharging the electrical load for the theoretic operation without storage is calculated using the fit of the measured reference EER data of chapter 2.2. The electrical load is calculated by equation 5b. The required input parameter $\dot{Q}_{Evap,Load}$, ambient temperature and part load ratio are measured respectively calculated constantly.

The PCM-storage was operated according to the strategy “maximized self-consumption”. All type days show a short discharging operation in the morning hours. The main part of storage discharge occurs in the late afternoon, when PV yield drops and the cooling load reaches its peak. The PV surplus energy available from about 10:00 is used to charge the storage instantly.

**Table 4: System data to compare the operation with and without PCM-storage for different type days.**

| Type day comparison | Type day 1 | | Type day 2 | | Type day 3 | | Type day 4 | |
|---|---|---|---|---|---|---|---|---|
| | PCM | no PCM | PCM | no PCM | PCM | no PCM | PCM | no PCM |
| Electrical load $E_{Cons,Sys}$ [kWh] | 50,3 | 51,2 | 50,8 | 50,2 | 39,5 | 39,7 | 36,5 | 36,2 |
| PV yield $E_{Gen,PV}$ [kWh] | 48,5 | 48,5 | 43,9 | 43,9 | 43,5 | 43,5 | 31,6 | 31,6 |
| Thermal load $Q_{evap,Load}$ [kWh] | 160,5 | 160,5 | 160,5 | 160,5 | 122,9 | 122,9 | 111,3 | 111,3 |
| Storage charging $Q_{Charge}$ [kWh] | 14,7 | -- | 16,7 | -- | 12,6 | -- | 14,7 | -- |
| DEER, 24 hours [-] | 3,19 | 3,13 | 3,16 | 3,20 | 3,12 | 3,10 | 3,05 | 3,08 |
| Autarky rate [%] | 80 | 74 | 71 | 67 | 76 | 70 | 66 | 62 |
| Self consumption rate [%] | 84 | 78 | 83 | 76 | 69 | 64 | 77 | 71 |

All type days of Table 4 have similar effects in common. In case of storage usage a higher thermal energy content is generated ($Q_{Evap,Load}$ + $Q_{Charge}$) compared to the case without PCM-storage. Nevertheless the entire electrical energy consumption $E_{Cons,Sys}$ is almost equal or even slightly lower (type day 1 and 3) compared to the reference. The storage energy content charged on a daily basis is returned to the system properly. Storage operation used for the load shift can be regarded as free of charge.

Applying solar operation the storage increases the systems autarky as well as the self-consumption rate for all 4 type days. Autarky improves in the range of 4 to 6%. Self-consumption is rising in the range of 5 to 7%.

The measured data of Figure 5 shows furthermore potential for optimizing solar operation in terms of grid interaction. Especially for type day 1 and 3 the grid feed-in, right after charging is finished, is quite high. Charging could have been delayed without any loss of solar fraction. To optimize operation, in a next step the predictive control described in chapter 2.4 has been implemented to the storage control strategy.

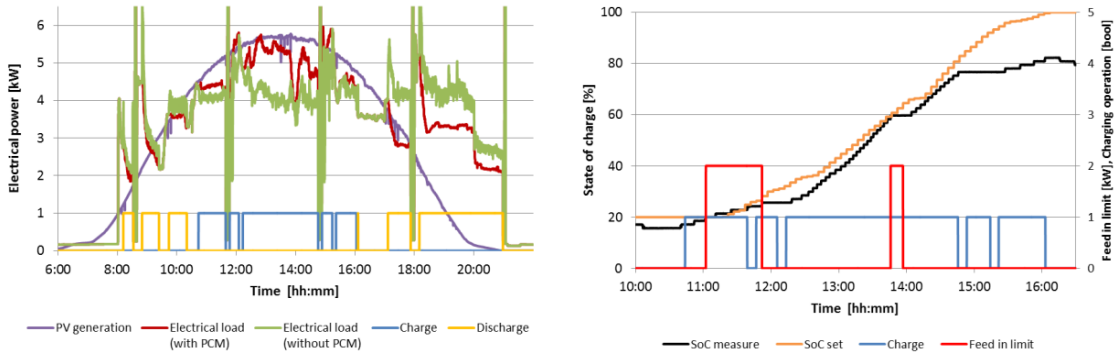


**Figure 6: Electrical data type day 1. Predictive control strategy implemented. Daily trend left. $SoC_{set}$ vs. $SoC_{measure}$ on the right.**

Figure 6 (left) shows the previously introduced electrical trend line. The daily trend is classified as type day 1. Yet, as a result of the predictive control, storage charging lasts longer in comparison to type day 1 shown in Figure 5, although nearly the same amount of thermal energy is charged. Thermal charging capacity is held back and the electrical load is matched more properly to the course of the PV peak than shown before for the strategy "maximized self-consumption". Nevertheless, storage charging is finished before discharging potential occurs. That means the usable PV self-consumption rate is entirely exploited, allowing for minimum of grid interaction.

The right side of Figure 6 shows details of the charging process. The orange line represents the calculated $SoC_{set}$, applying recorded data according to equation 9-11. In this case, for the parameter λ an average value of 0.3 has been chosen. The black line represents the currently measured SoC. The initially described distinction of cases, derived from a comparison of $SoC_{set}$ and $SoC_{measure}$ is applied. When system operates in "peak shaving" mode, for the switch back to "max. self-consumption" a hysteresis is implemented. The charging process starts, when the measured SoC is below $SoC_{set}$. Thus, at the very beginning charging is done by the strategy "max. self-consumption". Soon $SoC_{measure}$ overtakes $SoC_{set}$. Consequently, the controller set-point of allowed grid feed-in (red line, second y-Axis) is set from 0 to 2 kW. From now on charging is done in "peak shaving" mode with reduced power. Later on, when $SoC_{set}$ overtakes $SoC_{measure}$ again, the feed-in limit is set back to 0 kW. At 13:30 the same process is repeated. At the end of charging at 16:00 the measured SoC value reaches 82%. Nevertheless storage charging is completely done and the storage is fully charged. Here the limitation of the SoC determination becomes obvious, caused by the limits of the measurement procedure as described in section

2.4 (eq. 12).

The predictive control strategy works reliable and shows promising data. For a valid comparison to the basic strategy “max. self-consumption” more data have to be collected and analyzed. This topic shall be object of a further publication.

3.5. Grid orientated system operation

System cooling operation from 17th of April to 31st of July is evaluated. The distribution of electrical power data for the system demand, PV generation and remaining grid interaction is shown in Figure 7. Data were taken either when the system was in cooling mode or the PV generator was working. For 90% of the entire operation the storage charging strategy „max. self-consumption“ was applied.

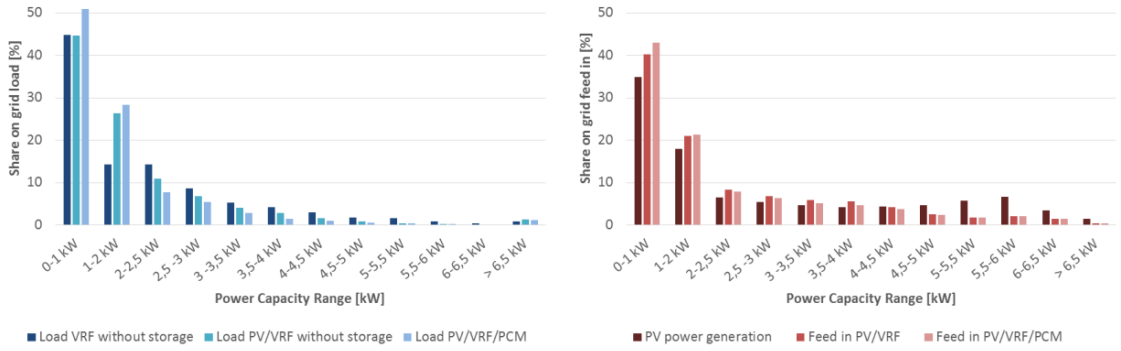


**Figure 7: Distribution of grid interaction power ratios. Left diagram: System load without storage (dark blue, 1st column), remaining grid load of PV/VRF (blue, 2nd column), remaining grid load of PV/VRF/PCM (light blue, 3rd column). Right diagram: PV generation (dark red, 1st column), remaining feed in PV/VRF (red, 2nd column), remaining feed in PV/VRF/PCM (light red, 3rd column). Cooling operation from 17th of April to 31st of July 2019.**

Figure 7 (left) shows data regarding grid load. The first column (dark blue) represents the load distribution of the entire VRF system without storage. The second column (blue) shows the same data when PV and VRF are coupled. The coupling of PV/VRF shows already a notable shift of the remaining grid load to lower power ranges. Over 80% of the remaining load is fulfilled by operating states below 2.5 kW. The last column (light blue) represents the load distribution for the entire system of PV/VRF and PCM. Utilization of the storage further increases the occurrence of lower power values. Running the PCM storage, 80% of remaining grid load is limited to a maximum of 2 kW. 95% of remaining grid load is limited to a power range below 3.5 kW.

The right side of Figure 7 shows data regarding grid feed in. The first column (dark red) shows the power distribution of the entire PV generation. The second column (red) shows the remaining feed in after the coupling of PV and VRF system. The coupling PV/VRF leads to a share of 90% of remaining grid feed in below 4.5 kW (PV-Installation: 7.2 kWp). The last column (light red) represents the feed in distribution for the entire system of PV/VRF/PCM. By utilization of the storage an additional but very slight shift towards lower power states is accomplished. The applied storage charging strategy „max. self-consumption“ does not significantly change the load distribution towards lower values. Especially when regulations regarding allowed power feed-in to the grid are getting stricter, this aspect will gain importance to avoid losses of the PV generation. Here the described and implemented predictive control strategy should lead to a notable improvement.

A well designed coupling of PV/VRF/PCM is able to ensure a grid-friendly system operation. To achieve this, it is mandatory to define balanced target values of both solar key parameters, autarky and self-consumption rate.

## 4. Summary and Outlook

A latent heat storage based on PCM has been integrated successfully in a VRF air-conditioning system, allowing for a substantial temporal load shift. Storage charging is done without any losses in cycle efficiency. For low part load ratios the storage charging is able to stabilize system operation, which leads to a favorable side effect. Storage discharge leads to a boost of the systems EER in the range of 27 to 10%, allowing a lower electrical demand when appropriate. For low part load ratios an increase of the EER by at least 20% is accomplished. For mean part load ranges the effect on the efficiency is comparatively low. The EER is boosted by 10 to 16%. The conventional VRF system with a pair of air heat exchangers acting as condensers is operating already quite efficiently. Especially for high part load operation, usually induced by high ambient temperatures, when the conventional system is struggling for efficiency, the use of the latent heat storage yield an improvement of the EER of 20 to 27%. This situation represents the target use case for which the latent heat storage had been designed for.

Solar-oriented operation of the storage leads to a rise of both solar key parameters, autarky and self-consumption rate. For different type days an improvement of autarky from 4 to 6% have been proven. Self-consumption rate can be raised by 5 to 7%. Precondition is a sufficient PV-yield for charging the storage. In terms of grid interaction the storage is able to move remaining systems grid demand towards lower power ranges. For remaining grid feed in, the storage use by now only leads to a slight shift towards lower power values. The control strategy “max. self-consumption” does not substantially reduce the occurrence of feed-in peaks. For this purpose a “peak shaving” mode has been integrated in the control strategy. Especially when future restrictions regarding allowed PV power feed-in are getting stricter, this aspect will gain further significance. Here, the successfully implemented predictive control strategy shows a significant potential. For a reliable assessment of the improved strategy, more practical data need to be recorded and analyzed.

For a profound economical assessment of the storage, further data of operation need to be collected. By now, trends can be pointed out: For areas with cooling load all year round, the storage use has a high potential. For regions with almost an even distribution between cooling and heating load around the year, the storage needs to fulfil heating purposes as well. In heating mode the storage is able to work as an efficient heat source in times of low ambient temperature conditions. This additional use will be necessary in order to increase the utilization rate of the storage, a prerequisite for economic operation.

## 5. Acknowledgments

The project SolarSplit is funded by the BMWi (German Federal Ministry for Economic Affairs and Energy) under grant No. 0325900 A, B and C.

## 6. References

Braam, F., Hillinger, R., Llerena Engesser, M., Müller, S., Kohrs, R., Wittwer, C., Peak Shaving with Photovoltaik-Battery Systems, 2014. IEEE PES Innovative Smart Grid Technologies, Istanbul.

Helm, M., Hagel, K., Pfeffer, W., Hiebler, S., Schweigler, C., 2013. Solares Heizen und Kühlen mit Absorptionskältemaschine und Latentwärmespeicher, Project „SolCool“ . FKZ 0329605O. https://opac.tib.eu/DB=1/XMLPRS=N/PPN?PPN=83277569X

Korth, T., Loistl, F., Storch, A., Schex, R., Krönauer, A., Schweigler, C., Latent heat storage for direct integration in the refrigerant cycle of an air conditioning system, 2018. HPC, Bayreuth, Germany.

Schex, R., Krönauer, A., Remy, M., Linn, J., Korth, T., Loistl, F., Schweigler, C., 2017. Solar-electric driven Heating and Cooling System with PCM-storage for improved Grid Connection, SHC Conference, Abu Dhabi.

Swegon Germany GmbH, 2014. https://www.swegon.com/de/produkte/kuhlen--heizen/fujitsu-vrf/fujitsu-airstage-ausseneinheiten/fujitsu-airstage-v-ii-r/

Weniger, J., Bergner, J. Tjaden, T., Quaschning, V., 2015. Dezentrale Solarstromspeicher für die Energiewende. Hochschule für Technik und Wirtschaft Berlin.